Charge state modification in Mn site substituted CMR manganites: strong deleterious influence on the ferromagnetic–metallic state

2007 J. Phys.: Condens. Matter 19 236207

(http://iopscience.iop.org/0953-8984/19/23/236207)

IOP PUBLISHING JOURNAL OF PHYSICS: CONDENSED MATTER

J. Phys.: Condens. Matter **19** (2007) 236207 (22pp) doi:10.1088/0953-8984/19/23/236207

Charge state modification in Mn site substituted CMR manganites: strong deleterious influence on the ferromagnetic–metallic state

L Seetha Lakshmi[1,2,3], K Dörr[2], K Nenkov[2], V S Sastry[1] and K-H Müller[2]

[1] XS & CGS, Materials Science Division, Indira Gandhi Centre For Atomic Research, Kalpakkam, Tamil Nadu 603102, India
[2] Institute of Metallic Materials, IFW Dresden, Postach 270116, Dresden 01171, Germany

E-mail: slaxmi73@gmail.com

Received 19 December 2006, in final form 19 April 2007
Published 8 May 2007
Online at stacks.iop.org/JPhysCM/19/236207

Abstract

The effect of charge state modification at the Mn site on the physical properties of CMR manganites is reported. With a view to avoiding additional complexity of local spin coupling effects, Mn site substitution of $La_{0.67}Ca_{0.33}MnO_3$ is carried out with appropriate diamagnetic ions—Zn^{2+}, Zr^{4+}, Ta^{5+} and W^{6+}—of different valence states. The substitution results in size changes of the unit cell and enhanced local structural distortions, which increase in the order Zn, Zr, Ta and W. The ground state is ferromagnetic–metallic below a certain critical concentration x_c of the substituents, beyond which the magnetic ground state shows a glassy behaviour. The phase transition temperatures (T_{MI} and T_c) decrease with substitution, but to different extents. The observed suppression rates of the Curie temperature, T_c, of ~39 K/at.% and ~45 K/at.% respectively for Ta^{5+} and W^{6+} substituted compounds are the highest reported in the Mn site substituted CMR manganites. Besides the modification of majority carrier concentration due to the increased (decreased) Mn^{3+} concentration and enhanced local structural effects, the local electrostatic potential of the substituents seems to contribute to the unusually strong reduction in the itinerant ferromagnetism and the observed glassy states.

1. Introduction

The discovery of colossal magnetoresistance (CMR) in thin films of mixed-valent $La_{0.67}Ca_{0.33}MnO_3$ has brought out a renaissance of research activities focused on the complex physical properties of the ortho-manganites [1] and realization of new functional materials. Their remarkable interplay of transport and magnetism [2] originates from the mixed valence

[3] Author to whom any correspondence should be addressed.

state of Mn—Mn^{3+} and Mn^{4+}; the latter arises to balance the charge deficit from the divalent Ca substitution. The CMR effect appears about at a temperature where the system undergoes an insulator–metal transition (at T_{MI}) with a simultaneous appearance of a para- to ferromagnetic transition (at T_c) at about 270 K [3]. Zener had proposed the double-exchange (DE) model to explain the concurrent occurrence of ferromagnetism and metallic transport in these compounds [4]. However, subsequent studies have shown that much still remains to be understood about the structure–property correlations [5, 6] and especially the complex nature of the interplay between the various degrees of freedom in these systems. These studies have highlighted the significance of strong electron–phonon coupling arising due to the Jahn–Teller distortion associated with the Mn^{3+} ion [7] and the complex charge/orbital ordering phenomena in the (La, Ca)MnO_3 system [8]. There was growing evidence to suggest that the DE model is insufficient to account for the rich variety of phenomena found in these compounds [9–12]. Subsequent studies have shown that previous proposals such as the polaron model [6] and Anderson localization [13, 14] were far from adequate to provide a realistic explanation of the complex ground state properties. Enormous efforts on experimental and theoretical fronts have converged on the idea that manganites are intrinsically inhomogeneous at various length scales [15, 16] and the complex ground state properties arise due to a strong interplay of the lattice, spin, charge and orbital degrees of freedom [17, 18]. Recent studies suggest that colossal effects are caused by competitive magnetic interactions in the background of disorder effects. Hence, the studies addressing the disorder effects are of current interest and experimentally this can be achieved by a suitable substitution at the La and/or Mn site. Furthermore, the phase-segregated state with glassy characteristics [19] challenges the current understanding of the system and many more exciting results are sure to unfold in the near future.

Extensive studies on La site substitutions with rare-earth ions of different sizes, Y [5, 20] Dy [21], Tb [22] etc, show that the lattice distortions introduced by La-site disorder influence the DE interaction strength by changing the Mn–O–Mn bond angle. Furthermore, the competition with antiferromagnetic super-exchange interactions may give rise to magnetically disordered states. It is important to note that this type of disorder indirectly affects DE interaction strength mediated through the Mn ions. The variation of the physical properties with rare-earth site substitution has been parametrized through the average ionic size of the La site ($\langle r_A \rangle$), often expressed as the Goldschmidt tolerance factor t given by $(\langle r_A \rangle + r_O)/\sqrt{2}(\langle r_{Mn} \rangle + r_O)$, where $\langle r_{Mn} \rangle$ and r_O are the average manganese and oxygen ionic radius respectively [23]. It was shown in the subsequent studies that a more general description requires the use of an additional parameter, the La-site size variance, $\sigma^2 = \langle r_A^2 \rangle - \langle r_A \rangle^2$ [24]. It is shown by Rodriguez *et al* [25] that at a fixed doping level ($x = 0.3$) and constant $\langle r_A \rangle$ the metal–insulator transition temperature shows a systematic linear decrease with an increase of σ^2 [26]. Above the critical dopant concentration, the lattice disorder leads to glassy characteristics in the ground state [21, 27, 28]. In these systems, evidence for clustering effects has also been reported [29]. Another important observation is that for a given value of carrier density (n), the bandwidth (W) could be fine tuned to a wide ((La–Sr)–Mn–O system), narrow ((Pr–Ca)–Mn–O system) or intermediate ((La–Ca)–Mn–O system) value through the variation in the parameters, average Mn–O bond length ($\langle d_{Mn-O} \rangle$) and average Mn–O–Mn bond angles ($\langle$Mn–O–Mn$\rangle$) [15]. Williams *et al* [30] have explored the role of yet another important factor, namely the charge disorder ($\sigma^2(q_A)$) effects on the physical properties of the rare-earth site substituted manganites. After an empirical scaling to correct for the residual lattice effects, it was shown that local charge variations are effectively screened in the La site substituted manganites. This study demonstrates that the effect of random electrostatic potential due to the differences in the formal charge between La site substituted ions have no significant effect on the transition temperatures [30, 31]. In contrast, charge state modification at the Mn site, that

forms the basis of the present study, is found to have a dramatic effect on the physical properties of the CMR manganites.

Since the essential degrees of freedom are closely linked to the Mn ions, substitution study at the Mn site is expected to bring about a dramatic effect. While the RE-site substitution studies had brought out the valuable structure–property correlation, they had left one of the ingredients of the DE interaction unexplored, namely the nature of local magnetic coupling between the neighbouring spins. This can only be addressed by Mn site substitution studies. A large number of studies have reported the effect of Mn site substitution on the physical properties of different manganite systems. Generally, it was found that possible substitutions by various ions such as 3d transition metals [32–37], Al [38, 39], In [40], Ga [41], Sn [42] and Ge [43] lower the phase transition temperatures, but to different extents, and eventually lead to insulating states exhibiting cluster/spin-glass properties. The reduction in the phase transition temperatures has been broadly attributed to the weakening of the DE interaction strength. No systematic attempts have been made to delineate the various factors affecting the transition temperatures. In our previous work, it was shown that there are at least two major contributions, (i) local structural effects and (ii) local magnetic coupling effects, influencing the transition temperatures of the CMR manganites [44], and local structural effects play a dominant role both in affecting the phase transition temperatures and in the ground state properties of CMR manganites. It was also hypothesized that local ferromagnetic coupling between the paramagnetic spins partially compensates the structural effects and enhances the DE interaction strength [45].

This study addresses the significance of yet another contribution, namely, the charge state modification effects at the Mn site on the physical properties of the CMR manganites. A suitable choice of substituents at the Mn site is necessary to delineate this effect. With this notion, substitution studies have been carried out with diamagnetic Zn, Zr, Ta and W ions differing in the valence state. With all these ions being diamagnetic owing to the closed shell nature, additional complexity of the local magnetic coupling effect is not expected. From the inter-comparison of the structural, electrical transport and the magnetic properties of the substituted compounds, it is proposed here for the first time that the charge state modification at the Mn site is the most deleterious for the physical properties of the Mn site substituted CMR manganites.

2. Experimental details

Bulk polycrystalline $La_{0.67}Ca_{0.33}Mn_{1-x}M_xO_3$ compounds, where M = Zn, Zr, Ta and W and $0 \leqslant x \leqslant 0.10$, were prepared by standard solid state reaction using stoichiometric amount of precursors, La_2O_3 (Indian-Rare-Earths), $CaCO_3$ (Cerac), MnO_2 (Cerac) and the respective transition metal oxides, ZnO, ZrO_2, Ta_2O_5 (Johnson Matthey) and WO_3 (Fluka), all with purity better than 99.995%. Care was taken to remove the moisture in La_2O_3 before weighing by preheating at 800 °C for 24 h. High purity acetone was used as a wetting medium to assist the mixing process of the precursors. The homogenized, dried powder was calcined at 980 °C for 24 h and subsequently ground and compacted into pellets of 15 mm diameter. The pellets were heat treated in the temperature range 1200 to 1475 °C for 72 h with four intermediate grindings followed by compaction steps. Pellets were further ground into very fine powder and compacted into pellets of 15 mm diameter and ∼1.5 mm thickness for various studies. Polyvinyl acetate (PVA) (2 wt%) solution was used as a binding material to improve the inter-grain connectivity. The final sintering in a single batch of each series of compounds was carried out at 1525 °C for 24 h in air. Sufficient care was taken that the preparation history is the same for all batches prepared. The typical density of the sintered pellets, determined by a modified

Archimedes method using ethanol as the liquid, was ∼92–95% of the theoretical density, and no systematic variations were observed with the composition of the substituent.

The high statistics room temperature powder x-ray diffraction (XRD) pattern in Bragg–Brentano para-focusing geometry with high statistics ($\sim 10^5$ counts over a dwell time of 25 s at the 100% peak) was recorded using Cu Kα radiation (STOE, Germany). Si powder (NIST SRM-640b) was used as an external standard for 2θ (zero) correction before recording each new set of XRD patterns. Analysis of the powder pattern to extract the crystallographic information was carried out using the GSAS Rietveld refinement program [46]. The SPUDS program was used for generating the starting model for the Rietveld analysis [47]. For all compounds, the site occupancy, taking the valence state of the constituting elements into account, was constrained to be consistent with the nominal stoichiometry of the compound. The atomic co-ordinates and isotropic thermal parameters were constrained to be equal for the different atomic species having the same point symmetry. They were allowed to vary independently for different compositions of the substituents. The resistivity measurements ($\rho(T)$) in zero and in 7 T field were performed on rectangular bar shaped pellets by the conventional four-probe method using a Maglab^{1992} system (Oxford Instruments, UK). A superconducting spilt coil magnet was employed for steady magnetic fields up to 7 T with the magnetic field parallel to the current. The magnetoresistance (MR) is estimated using the relation $\mathrm{MR}(\%) = ((\rho_{H\neq 0} - \rho_{H=0})/\rho_{H=0}) \times 100$ where $\rho_{H\neq 0}$ and $\rho_{H=0}$ denote the resistivity in the presence and absence of the magnetic field respectively. To study the MR as a function of field, samples were cooled in zero field condition to 5 K. The magnetic field was swept from 0 to +7 T to 0 to −7 T and then back to 0 T and resistance was recorded along the field sweep. The temperature variation of ac susceptibility with an ac probe field (h) of 1 Oe and an excitation frequency (f) of 133 Hz was measured using a Lakeshore 7000 series susceptometer. The samples were cooled in ZFC condition to 4.2 K and the data were collected in the warming mode.

The reported metal to insulator transition (MIT) temperature (T_{MI}) is the temperature corresponding to the maximum in the electrical resistivity. The Curie temperature (T_{c}) of the compounds is estimated from the in-phase component of ac susceptibility ($\chi'(T)$) by a tangent method.

3. Experimental results

3.1. Room temperature powder x-ray diffraction

Figures 1(a)–(d) show the high statistics room temperature powder x-ray diffraction (XRD) patterns of $La_{0.67}Ca_{0.33}Mn_{1-x}M_xO_3$ ($0 \leqslant x \leqslant 0.10$) compounds (where M = Zn, Zr, Ta and W). All the compounds, except W substituted compounds with $x \geqslant 0.05$, are mono-phase in nature. The entire diffraction pattern could be indexed to the orthorhombic $Pnma$ space group (space group no 62). Rietveld refinement yielded an excellent agreement between the observed (I_{obs}) and calculated (I_{cal}) diffraction profiles with no peaks left un-indexed, confirming the fact that the compounds are single phase. As a representative of each series, the Rietveld fitted XRD patterns of $La_{0.67}Ca_{0.33}MnO_3$ (undoped), $La_{0.67}Ca_{0.33}Mn_{0.90}M_{0.10}O_3$ (M = Zn, Zr and Ta) and $La_{0.67}Ca_{0.33}Mn_{0.97}W_{0.03}O_3$ compounds are displayed in figure 2. The XRD patterns of W substituted compounds with $x \geqslant 0.05$ show some additional peaks. To explore a possible structural transition to monoclinic symmetry, whole pattern fitting to $P21/c$ symmetry (space group no 14) and $P21/m$ symmetry (space group no 11) were attempted but without success. In an attempt to form single-phase compounds, these samples were further heat treated in the temperature range 1550–1685 °C for 12–24 h in flowing oxygen with intermediate grinding

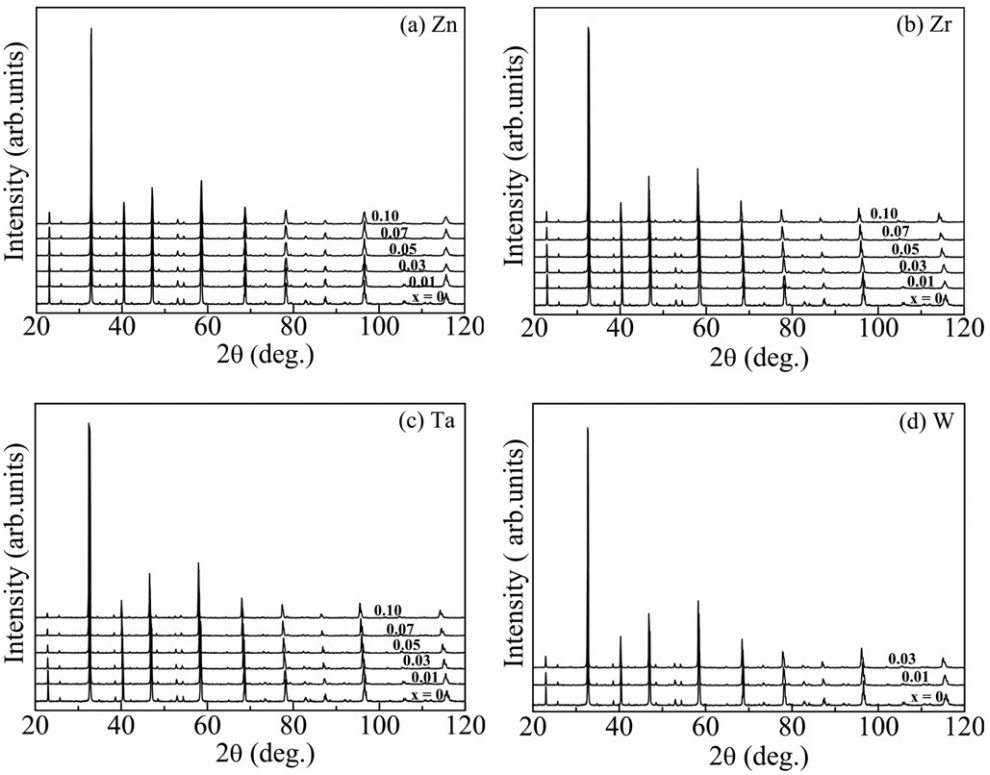

Figure 1. High statistics room temperature powder x-ray diffraction patterns of $La_{0.67}Ca_{0.33}Mn_{1-x}M_xO_3$ ($0 \leqslant x \leqslant 0.10$) compounds where (a) M = Zn, (b) Zr, (c) Ta and (d) W.

and pelletization. The RT XRD patterns after each step of high temperature annealing contain the additional peaks corresponding to an unidentified phase and Mn_3O_4. This indicates that the solubility for W^{6+} with the present synthesis procedure under ambient pressure is limited to $x = 0.03$. From the integrated intensity analysis of the reflections observed in the limited 2θ ranges 28°–36° and 44°–55°, the volume fraction of unidentified phase and Mn_3O_4 for $x = 0.05$ is determined to be ∼15% and 10% respectively. Their volume fraction is found to increase with W concentration. Further characterization studies and discussions for the W substituted system are therefore, limited to single phase compounds with $x \leqslant 0.03$.

The refined lattice parameters (a, b and c) and unit cell volume (v), reliability factors (R_{wp} and R_p) and goodness of fit (S) are tabulated in tables 1–4. The composition dependences of a, b and c and v and also $\langle d_{Mn-O}\rangle$ and ⟨Mn–O–Mn⟩ estimated from the refined atomic positions are shown in figures 3 and 4 respectively. As seen in figure 3, all the substituents vary the unit cell parameters almost linearly in the entire range of substitution. Whereas Zr substitution results in a significant increase (figure 3(b)), Zn having the same ionic radius (IR) results in a marginal decrease in the unit cell parameters (figure 3(a)). For instance, for $x = 0.10$ of Zr (Zn), an increase (decrease) in a, b and c and v of 0.9 (−0.02), 0.9 (−0.02), 0.6 (−0.005) and 2.5 (−0.05)% respectively are observed. On the other hand, pentavalent Ta, despite having an IR close to that of Mn^{3+} ion, and hexavalent W, having a smaller IR than Mn^{3+}, introduce an appreciable increase in the unit cell parameters. For instance, for the highest level of Ta substitution ($x = 0.10$), increases in a, b and c and v of 0.9, 0.8, 0.5 and 2.3%

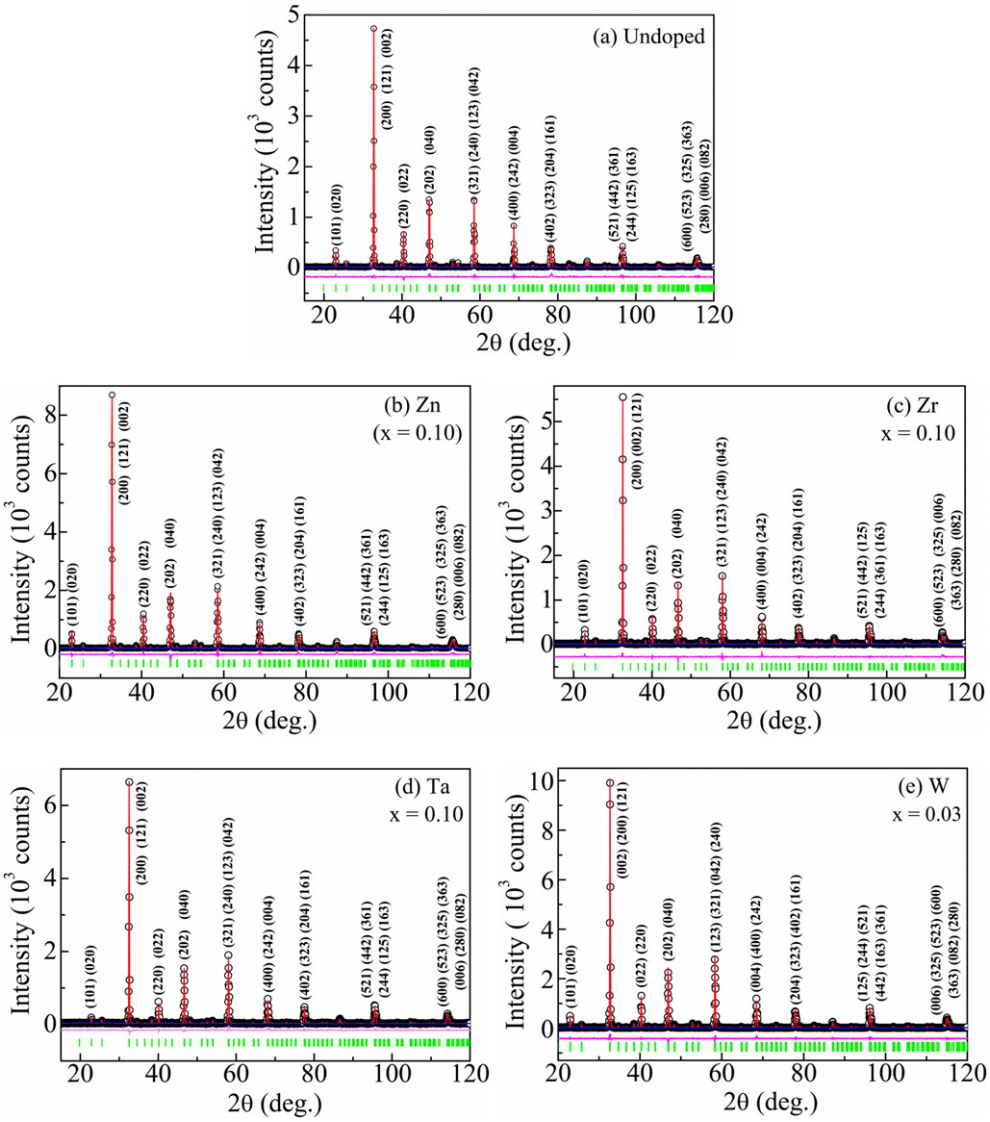

Figure 2. (a) Rietveld refinement spectrum of $La_{0.67}Ca_{0.33}MnO_3$ (undoped) compound. As a representative of the series, similar spectra of $La_{0.67}Ca_{0.33}Mn_{0.90}M_{0.10}O_3$ where (b) M = Zn, (c) Zr (d) Ta and (e) $La_{0.67}Ca_{0.33}Mn_{0.97}W_{0.03}O_3$ compounds are also shown. In each spectrum, the symbol denotes the observed intensity (I_{obs}); the continuous line denotes the calculated intensity (I_{cal}). Difference between the observed and the calculated intensities are shown at the bottom of the figure. The calculated Bragg-reflected positions are marked by the vertical bars. The Miller indices of the major Bragg reflections are also indicated.

(This figure is in colour only in the electronic version)

respectively are observed (figure 3(c)). Also, for $x = 0.03$ of W substitution, an increase in unit cell parameters of 0.4, 0.3, 0.2 and 0.9% is found to be slightly larger than that of Ta of the same composition. For all substitutions except Zn, an elongation of $\langle d_{Mn-O} \rangle$ is apparent with increasing x. These results are consistent with the observed unit cell expansion (inset of

Table 1. The refined lattice parameters (a, b and c) (in Å), unit cell volume (v) (in Å^3), reliability factors (R_{wp}, R_p) and goodness of fit (S) from the Rietveld analysis of $La_{0.67}Ca_{0.33}Mn_{1-x}Zn_xO_3$ ($0 \leqslant x \leqslant 0.10$) compounds. Numbers in parenthesis indicate the standard deviation in the last digit.

	Lattice parameters (in Å)			Unit cell volume (v)	R-factors (in %)		
x	a	b	c	(in Å^3)	R_p	R_{wp}	S
0	5.4594(1)	7.7137(1)	5.4545(1)	230.543(4)	11.62	18.12	1.36
0.01	5.4595(1)	7.7132(1)	5.4541(1)	230.532(6)	10.96	15.43	1.48
0.03	5.4593(1)	7.7127(1)	5.4538(1)	230.509(4)	10.51	14.20	1.45
0.05	5.4590(1)	7.7126(1)	5.4537(0)	230.489(5)	9.14	13.22	1.33
0.07	5.4586(1)	7.7125(1)	5.4536(1)	230.464(6)	10.52	14.36	1.46
0.10	5.4584(1)	7.7121(2)	5.4533(1)	230.440(6)	8.16	11.37	1.28

Table 2. The refined lattice parameters (a, b and c) (in Å), unit cell volume (v) (in Å^3), reliability factors (R_{wp}, R_p) and goodness of fit (S) from the Rietveld analysis of $La_{0.67}Ca_{0.33}Mn_{1-x}Zr_xO_3$ ($0 \leqslant x \leqslant 0.10$) compounds. Numbers in parenthesis indicate the standard deviation in the last digit.

	Lattice parameters (in Å)			Unit cell volume (v)	R-factors (in %)		
x	a	b	c	(in Å^3)	R_p	R_{wp}	S
0	5.4594(1)	7.7137(1)	5.4545(1)	230.543(4)	11.62	18.12	1.36
0.01	5.4665(2)	7.7199(2)	5.4771(1)	231.138(5)	11.01	17.47	1.33
0.03	5.4729(1)	7.7332(1)	5.4826(1)	232.040(3)	11.06	17.30	1.44
0.05	5.4860(2)	7.7530(1)	5.4899(2)	233.502(5)	11.01	15.11	1.27
0.07	5.4969(1)	7.7647(1)	5.4962(2)	234.588(5)	10.54	14.87	1.28
0.10	5.5104(1)	7.7831(1)	5.5080(1)	236.227(3)	10.34	14.01	1.20

Table 3. The refined lattice parameters (a, b and c) (in Å), unit cell volume (v) (in Å^3), reliability factors (R_{wp}, R_p) and goodness of fit (S) from the Rietveld analysis of $La_{0.67}Ca_{0.33}Mn_{1-x}Ta_xO_3$ ($0 \leqslant x \leqslant 0.10$) compounds. Numbers in parenthesis indicate the standard deviation in the last digit.

	Lattice parameters (in Å)			Unit cell volume (v)	R-factors (in %)		
x	a	b	c	(in Å^3)	R_p	R_{wp}	S
0	5.4594(1)	7.7137(1)	5.4545(1)	230.543(4)	11.62	18.12	1.36
0.01	5.4665(1)	7.7233(1)	5.4783(1)	231.298(5)	11.62	16.47	1.27
0.03	5.4770(1)	7.7391(1)	5.4840(1)	232.455(5)	11.01	17.3	1.32
0.05	5.4879(1)	7.7532(1)	5.4908(1)	233.635(9)	11.05	16.22	1.29
0.07	5.4973(2)	7.7644(1)	5.4947(2)	234.538(5)	10.99	15.36	1.26
0.10	5.5091(1)	7.7772(1)	5.5025(2)	235.759(6)	10.24	14.35	1.22

figure 3). It is noteworthy that $\langle d_{Mn-O} \rangle$ (figure 4(a)) and $\langle$Mn–O–Mn$\rangle$ (inset of figure 4(a)) show a marginal decrease throughout the series of Zn substituted compounds (figure 3(a)). Hence, the Zn substituted series of compounds provides an example for vanishing structural modification by the substitution at the Mn site of $La_{0.67}Ca_{0.33}MnO_3$.

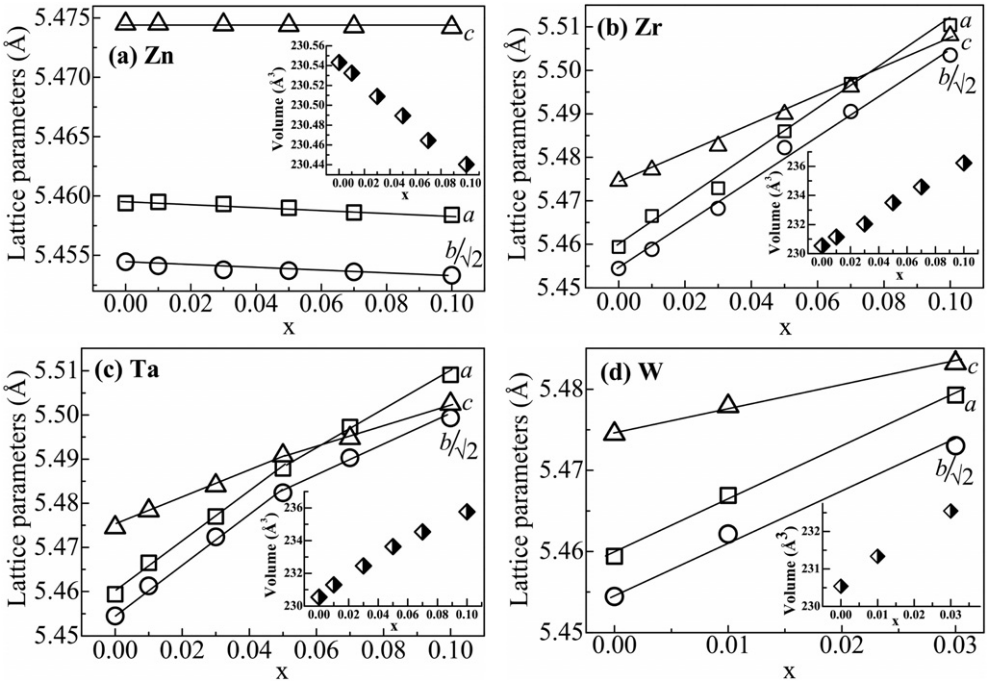

Figure 3. Composition (x) dependence of lattice parameters (a, b and c) and the unit cell volume (v) (inset) of $La_{0.67}Ca_{0.33}Mn_{1-x}M_xO_3$ ($0 \leqslant x \leqslant 0.10$) compounds where (a) M = Zn (b) Zr, (c) Ta and (d) W.

Table 4. The refined lattice parameters (a, b and c) (in Å), unit cell volume (v) (in Å^3), reliability factors (R_{wp}, R_p) and goodness of fit (S) from the Rietveld analysis of $La_{0.67}Ca_{0.33}Mn_{1-x}W_xO_3$ ($0 \leqslant x \leqslant 0.03$) compounds. Numbers in parenthesis indicate the standard deviation in the last digit.

	Lattice parameters (in Å)			Unit cell volume (v)	*R*-factors (in %)		
x	a	b	c	(in Å^3)	R_p	R_{wp}	S
0	5.4594(1)	7.7137(1)	5.4545(1)	230.543(4)	11.62	18.12	1.36
0.01	5.4669(1)	7.7246(1)	5.4779(1)	231.339(6)	11.49	15.33	1.31
0.03	5.4793(1)	7.7400(1)	5.4832(1)	232.547(5)	9.14	12.75	1.29

3.2. Resistivity

The substitutions are found to affect electrical transport behaviour to various extents (tables 5–8). First, except for $x = 0.10$ of Zn and Ta beyond $x = 0.03$, all compounds exhibit an MIT (figures 5(a)–(d)). For each series of compounds, except for Zr when $x = 0.10$, T_{MI} shifts towards lower temperature. Second, Zr^{4+} and W^{6+} exhibit an MIT in the entire range of substitution (figures 5(b) and (d)), whereas Zn^{2+} undergoes an MIT up to $x = 0.07$ and for $x = 0.10$ an insulating behaviour is observed over the entire temperature range of measurement (figure 5(a)). The Ta^{5+} substituted compounds beyond $x = 0.03$ show an insulating behaviour (figure 5(c)). Since our experimental set-up limits the resistivity measurement to 10^6 Ω cm, no data could be collected below ∼70 K for Zn ($x = 0.10$) and ∼100 K for $x = 0.05, 0.07$ and 0.10 for the Ta substituted compounds. Nonetheless, the samples were further cooled down

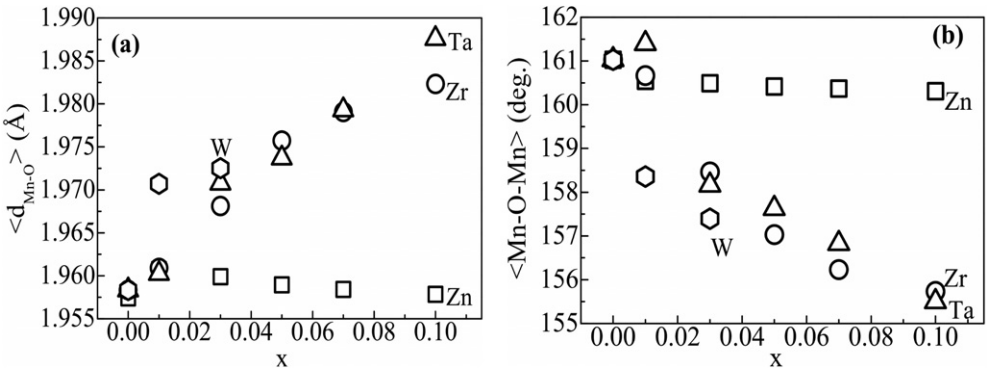

Figure 4. (a) The composition (x) dependence of average Mn–O bond length ($\langle d_{\mathrm{Mn-O}}\rangle$) and (b) average Mn–O–Mn bond angle ($\langle$Mn–O–Mn$\rangle$) of $La_{0.67}Ca_{0.33}Mn_{1-x}M_xO_3$ ($0 \leqslant x \leqslant 0.10$) compounds where M = Zn (□), Zr (○), Ta (△) and W (⬡).

Table 5. Metal–insulator transition temperature (T_{MI}) (in K) under a magnetic field, $H = 0$ and 7 T, Curie transition temperature (T_c) (in K), residual resistivity (ρ_0) (in Ω cm), polaron fit parameters: polaron hopping energy (E_{H}) (in meV) and pre-exponential factor (B) (in Ω cm K^{-1}), temperature corresponding to the maximum in magnetoresistance at 7 T (T_{MR}) (in K), magnetoresistance at the maximum in MR(T) under 7 T (MR_7) (in %) and grain boundary contribution to MR estimated from LFMR (GBMR) (in %) of $La_{0.67}Ca_{0.33}Mn_{1-x}Zn_xO_3$ ($0 \leqslant x \leqslant 0.10$) compounds.

	x					
Parameters	0	0.01	0.03	0.05	0.07	0.10
T_{MI}						
$H = 0$	266.6	257.6	221.5	134.5	101.7	No MIT
$H = 7$	>300	>300	252.2	155.5	125.3	63
T_c	268.9	261.1	226.3	139.5	110.4	$T_f = 45$[a]
ρ_0	0.053	0.068	0.072	0.928	6.0	142.6
E_{H}	—	150.7	152.5	154.8	—	—
$B \times 10^{-6}$		1.2	1.6	2.0	—	—
T_{MR7}	266.6	257.8	221.5	131.5	98.7	—
MR_7	63.8	62.7	74.8	91.1	98.5	—
GBMR	23.9	22.2	22.8	22.3	—	—

[a] T_f denotes the spin freezing temperature. Refer to text for details.

with frequent checks on the value of the resistivity, and such checks show that the resistivity of these compounds, even at 4.2 K, is beyond the measurable range, indicating the non-metallic nature of the compounds. In the high temperature paramagnetic–insulating regime, $\ln(\rho/T)$ versus $1/T$ curves for $x \leqslant 0.07$ follow a linear relation, indicating that the electrical transport is governed by thermally activated hopping of small polarons in the adiabatic limit [48]. On the other hand, for the compounds showing an insulating behaviour, the adiabatic small polaron model is not found to hold in the entire temperature range and is not considered for further discussion. The estimated polaron hopping energy (E_{H}) of all the series of compounds under consideration (tables 5–8) is consistently higher than that of the undoped compound [49], and except for Zr it increases with increasing x in the entire range of substitution, consistent with the previous report on Ga substituted $La_{0.67}Ca_{0.33}MnO_3$ [41]. The pre-exponential factor (B), except for Zr substituted compounds, shows a systematic linear increase with x. For Zr

Table 6. Metal–insulator transition temperature (T_{MI}) (in K) under a magnetic field, $H = 0$ and 7 T, Curie transition temperature (T_c) (in K), residual resistivity (ρ_0) (in Ω cm), polaron fit parameters: polaron hopping energy (E_H) (in meV) and pre-exponential factor (B) (in Ω cm K^{-1}), temperature corresponding to the maximum in magnetoresistance at 7 T (T_{MR}) (in K), magnetoresistance at the maximum in MR(T) under 7 T (MR_7) (in %) and grain boundary contribution to MR estimated from LFMR (GBMR) (in %) of $La_{0.67}Ca_{0.33}Mn_{1-x}Zr_xO_3$ ($0 \leqslant x \leqslant 0.10$) compounds.

	x					
Parameters	0	0.01	0.03	0.05	0.07	0.10
T_{MI}						
$H = 0$	266.6	239.6	197.5	128.5	86.1	95.5
$H = 7$	>300	281.0	230.2	182.5	68.4	83.3
T_c	268.9	236.1	200.9	130.8	126.8	125.9
ρ_0	0.053	0.032	0.092	4.2	124.1	147.9
E_H	—	151.4	163.3	176.2	174.1	173.9
$B \times 10^{-6}$	—	1.2	1.5	2.2	1.7	1.72
T_{MR7}	266.6	236.6	188.5	128.5	112	116.5
MR_7	63.8	78.3	80.5	92.8	92.7	89.5
GBMR	23.9	26.3	26.2	—	—	—

Table 7. Metal–insulator transition temperature (T_{MI}) (in K) under a magnetic field, $H = 0$ and 7 T, Curie transition temperature (T_c) (in K), residual resistivity (ρ_0) (in Ω cm), polaron fit parameters: polaron hopping energy (E_H) (in meV) and pre-exponential factor (B) (in Ω cm K^{-1}), temperature corresponding to the maximum in magnetoresistance at 7 T (T_{MR}) (in K), magnetoresistance at the maximum in MR(T) under 7 T (MR_7) (in %) and grain boundary contribution to MR estimated from LFMR (GBMR) (in %) of $La_{0.67}Ca_{0.33}Mn_{1-x}Ta_xO_3$ ($0 \leqslant x \leqslant 0.10$) compounds.

	x					
Parameters	0	0.01	0.03	0.05	0.07	0.10
T_{MI}						
$H = 0$	266.6	239.6	164.5	—	—	—
$H = 7$	>300	272.2	211.7	—	—	—
T_c	268.9	239.0	153.0	129.6	121.3	110.8
ρ_0	0.053	0.077	0.372	—	—	—
E_H	—	160.6	175.2	—	—	—
$B \times 10^{-6}$	—	1.27	1.87	—	—	—
T_{MR7}	266.6	239.6	161.5	—	—	—
MR_7	63.8	74.7	96.4	—	—	—
GBMR	23.9	24.6	24.9	—	—	—

substituted compounds, B rises with x up to $x = 0.05$ and then decreases for $x = 0.07$, and subsequently a marginal increase is observed for $x = 0.10$ (table 6).

Zn^{2+}, Zr^{4+}, Ta^{5+} and W^{6+} ions substituted in the octahedrally co-ordinated Mn site are not Jahn–Teller ions. Owing to a closed-shell electronic configuration, they act as a barrier to hopping due to their strong on-site Coulomb repulsion and thereby increase the average hopping distance (α). As will be shown subsequently, substitution of these ions modifies the relative concentration of Mn^{3+} and Mn^{4+} to preserve charge neutrality. Thus the two factors that alter B significantly are polaron concentration (n) and α [48]. For instance, whereas Zn^{2+} decreases the Mn^{3+} concentration, Zr^{4+} does not alter the Mn^{3+} concentration over the entire substitution range. On the other hand, Ta^{5+} and W^{6+} increase the relative concentration of Mn^{3+} ions in that order. If n is the dominant factor, B is expected to decrease as a function of x for Ta^{5+}

Table 8. Metal–insulator transition temperature (T_{MI}) (in K) under a magnetic field, $H = 0$ and 7 T, Curie transition temperature (T_c) (in K), residual resistivity (ρ_0) (in Ω cm), polaron fit parameters: polaron hopping energy (E_H) (in meV) and pre-exponential factor (B) (in Ω cm K^{-1}), temperature corresponding to the maximum in magnetoresistance at 7 T (T_{MR}) (in K), magnetoresistance at the maximum in MR(T) under 7 T (MR_7) (in %) and grain boundary contribution to MR estimated from LFMR (GBMR) (in %) of $La_{0.67}Ca_{0.33}Mn_{1-x}W_xO_3$ ($0 \leqslant x \leqslant 0.03$) compounds.

	x		
Parameters	0	0.01	0.03
T_{MI}			
$H = 0$	266.6	227.6	203.5
$H = 7$	>300	254.2	224.4
T_c	268.9	220.9	133.4
ρ_0	0.053	0.917	4.1
E_H	—	206.1	219.6
$B \times 10^{-6}$	—	2.40	3.90
T_{MR7}	266.6	224.8	191.4
MR_7	63.8	79.43	81.6
GBMR	23.9	30.7	30.3

and W^{6+} substituted compounds. Hence it is believed that, even at higher concentration of substituent, α might play a dominant role in affecting the electrical transport properties of the compounds.

3.3. Magnetoresistance

The effect of magnetic field of 7 T on the temperature dependence of resistivity of the compounds is also shown in figure 5. Two characteristic features clearly stand out. (i) An overall reduction in the resistivity over the entire temperature range and (ii) for metallic samples except for $x = 0.07$ and 0.10 of Zr, magnetic field causes a shift of T_{MI} to higher temperature and the maximum broadens. Notably, for $x = 0.10$ of Zn substituted compound, not only is the resistivity reduced under applied magnetic field, but also it exhibits an MIT with a $T_{MI} \approx 63$ K (figure 5(a)). In comparison, for Ta substituted compounds with $x \geqslant 0.03$, such an MIT could not be induced (figure 5(c)), and at as low a temperature as 4.2 K the resistivity of the compound is beyond the measurable range of the instrument, i.e. $\rho > 10^6$ Ω cm.

3.3.1. Temperature dependence of magnetoresistance. The temperature dependence of MR (MR(T)) of the substituted compounds for $\mu_0 H = 7$ T is shown in figures 6(a)–(d). For all the metallic samples except for $x = 0.07$ and 0.10 of Zr substitution, the maximum in MR occurs at a temperature (T_{MR7}) slightly lower than T_{MI} in the zero field resistivity (tables 5–8). For the two Zr substituted samples, T_{MR7} is at much higher temperatures than the respective T_{MI}. For $x = 0.10$ of Zn substituted compound MR monotonically increases, and at about 75 K an incipient peak-like feature is observed. Due to the non-availability of zero field resistivity data, MR could not be evaluated below 75 K and hence the presence of a maximum in the MR(T) curves could not be confirmed. The MR(T) curves of the insulating Ta compounds also exhibit an incipient peak-like feature, and here too the existence of apeak could not be confirmed owing to the non-availability of the zero field $\rho(T)$ data. In a given series, with MR(T) curves exhibiting a peak, it is observed that, excluding Zr substituted compounds, the MR at T_{MR7} increases with lowering of T_{MI}, i.e., the lower the T_{MI}, the higher will be the MR at T_{MR7}

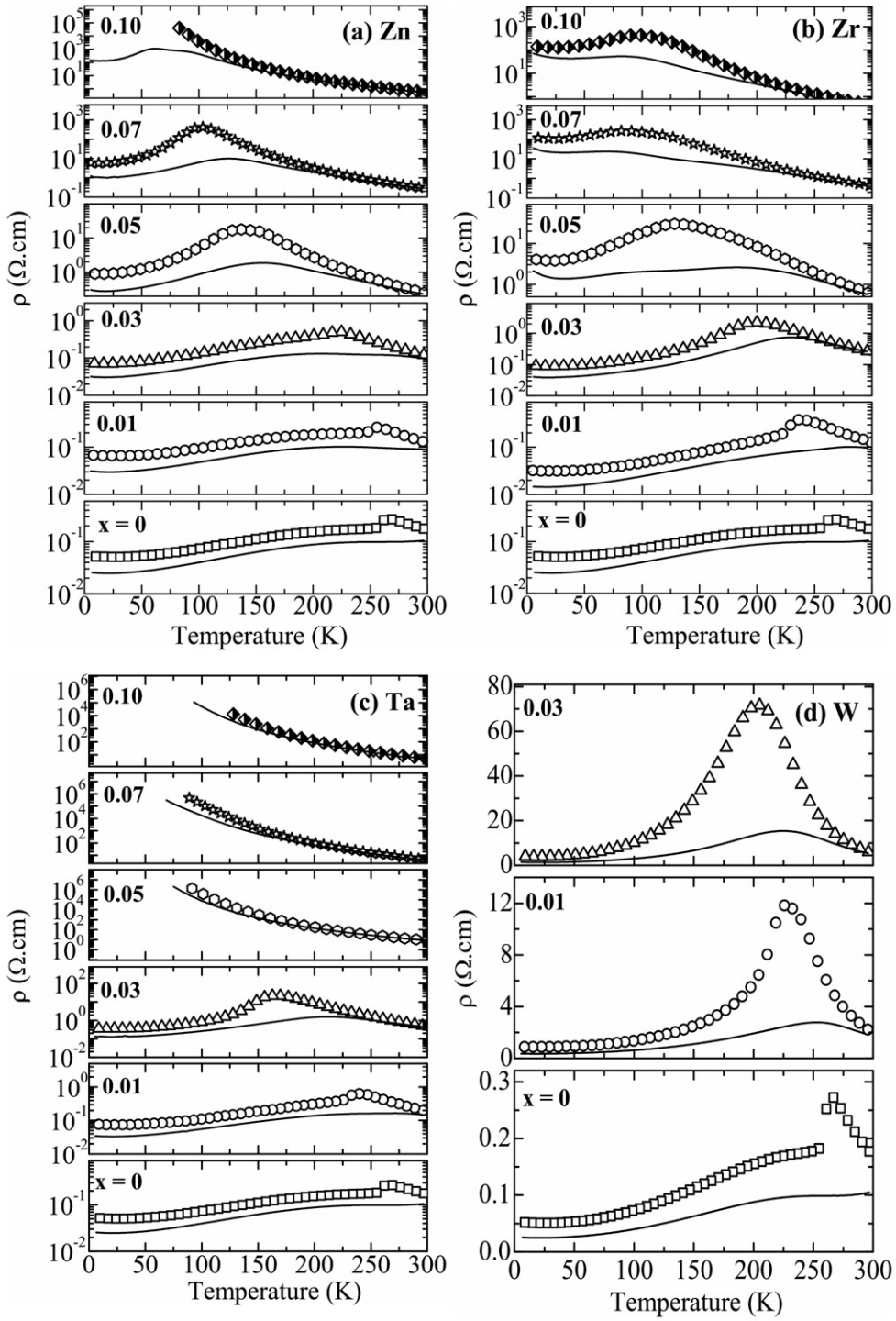

Figure 5. Temperature dependence of resistivity ($\rho(T)$) in the absence of magnetic field ($H = 0$) (symbols) and in 7 T (continuous line) field for $La_{0.67}Ca_{0.33}Mn_{1-x}M_xO_3$ ($0 \leqslant x \leqslant 0.10$) compounds where (a) M = Zn, (b) Zr, (c) Ta and (d) W.

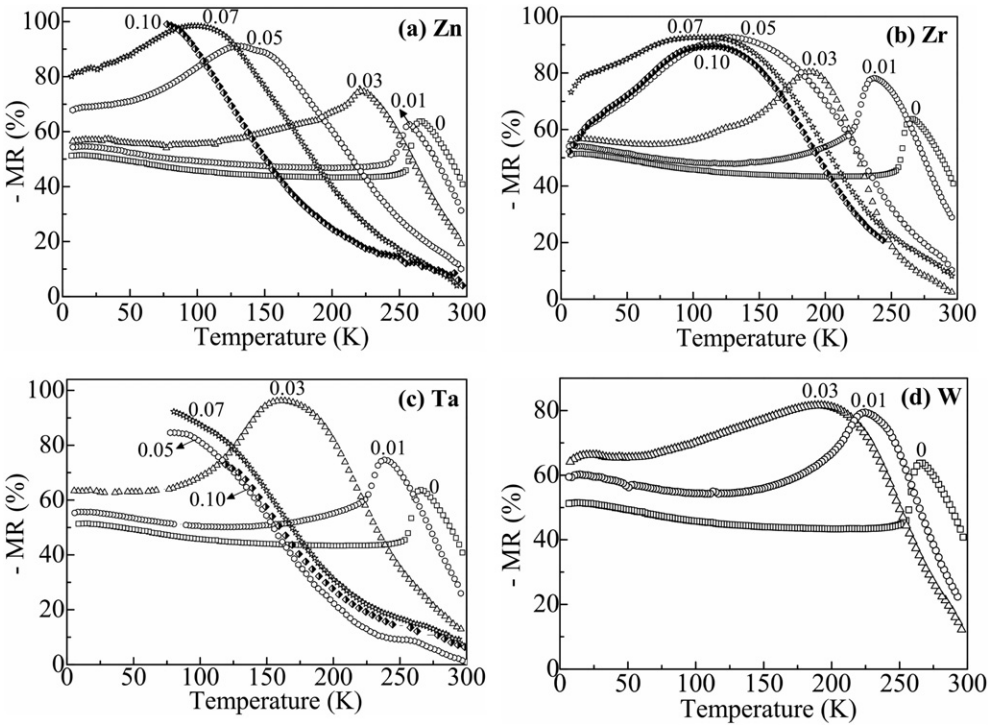

Figure 6. Temperature dependence of MR in a magnetic field of 7 T of $La_{0.67}Ca_{0.33}Mn_{1-x}M_xO_3$ ($0 \leqslant x \leqslant 0.10$) compounds where (a) M = Zn, (b) Zr, (c) Ta and (d) W.

(tables 5–8). Such behaviour has also been reported for the La-site substituted manganites. For the metallic compounds, the magnitude of MR maximum (MR_7) is found to increase with x. There is a significant MR away from the maximum, showing a weak temperature dependence on further lowering the temperature. This is attributed to spin-polarized tunnelling at the grain boundaries and is shown to be a characteristic feature of the polycrystalline manganites [50, 51].

3.3.2. Field dependence of magnetoresistance. Shown in figures 7(a)–(d) is the field dependence of MR of the substituted compounds at 5 K. For a lower level of substitution ($x \leqslant 0.03$), the MR response shows two distinct regions. The more pronounced drop appearing at low fields (<0.5 T) is attributed to the spin polarized tunnelling through grain boundaries and has been shown to be a characteristic feature of the polycrystalline manganites [50, 51]. When the field exceeds 0.5 T, the MR(H) response is found to have a much smaller slope. In ferromagnetic conducting manganites, this MR at higher magnetic field has been understood as a result of the field-induced ordering of magnetic moments inside the grain boundaries [52]. On the other hand, in phase separated manganites, this was understood in terms of the rotation of the domains along the field direction and/or the increase in the volume fraction of the ferromagnetic domains [17]. For $x \geqslant 0.05$, MR shows an almost linear dependence on μ_0H up to 7 T. Additional field cycling leads to large hysteresis and non-closure of MR at zero field (inset of figures 7(a)–(b)). It is worth noting that the value of MR non-closure at zero field increases with x. For instance, for $x = 0.10$ of Zr, it is found to be as high as 40%. Such behaviour is also reported in the insulating cobaltates [53] and it is attributed to the freezing of the clusters.

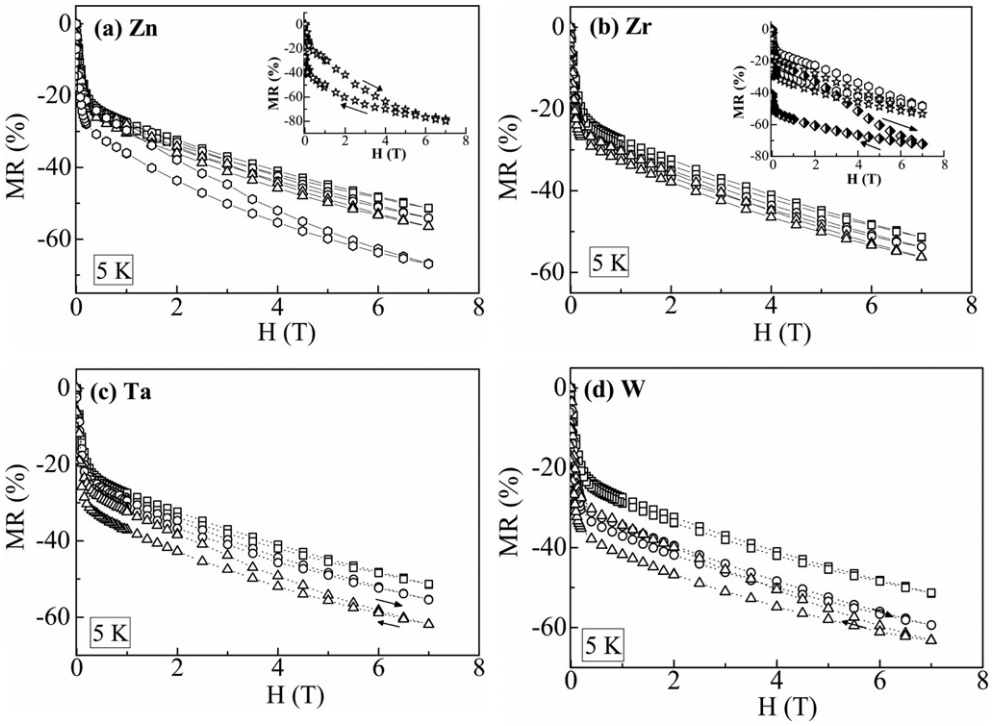

Figure 7. Magnetic field dependence of MR at 5 K of $La_{0.67}Ca_{0.33}Mn_{1-x}M_xO_3$ ($0 \leqslant x \leqslant 0.10$) compounds for $x = 0$ (□), 0.01 (○), 0.03 (△), 0.05 (⬡), 0.07 (☆) and 0.10 (◑) where (a) M = Zn (b) Zr, (c) Ta and (d) W. The inset of figures 7(a) and (b) shows the large hysteresis of MR of $x \geqslant 0.05$ with field cycling. The arrow indicates the direction of field sweep. Refer to the text for other details.

3.4. ac susceptibility

The $\chi'(T)$ curves (figures 8(a)–(d)) show that all the compounds, excluding $x = 0.10$ of Zn, undergo a para- to ferromagnetic transition. T_c of the substituted compounds decreases with substitution, but to different extents (tables 5–8). For the Ta and W substituted compounds, the observed reduction in T_c is found to be much larger than that of Fe^{3+} [54], Al^{3+} [38], Ga^{3+} [41], Ti^{4+} [32] and Ru^{4+} [45] substituted $La_{0.67}Ca_{0.33}MnO_3$. Another striking feature to note is that all the substituents, beyond a certain critical concentration (x_c), result in a cusp-like feature in χ' just below T_c. Additionally, except for Zn, a broad shoulder in χ' could be seen at lower temperatures. Interestingly, the cusp-like anomaly and the broad shoulder evolve into two distinct maxima under suitable static bias field: close to T_c and at low temperatures (T_g), marking the spin freezing temperature [55, 56]. While the high temperature maximum broadens and shifts to higher temperatures, the low temperature maximum shifts to lower temperatures with an increase in the bias field. Unlike the high temperature maximum, the latter low temperature maximum in the χ' signal exhibits a frequency dependent shift to higher temperatures [55]. A detailed discussion of the nature of the modified magnetic ground state is being published elsewhere [56]. In conjunction with the static response of the system, it is suggested that all the other compounds barring the Zn substituted one exhibit a cluster-glass (CG) state. The temperature dependence of the ac susceptibility of the Zn substituted compound is qualitatively similar to that of the $La_{0.67}Ca_{0.33}Mn_{0.9}Fe_{0.1}O_3$ compound [57]. In

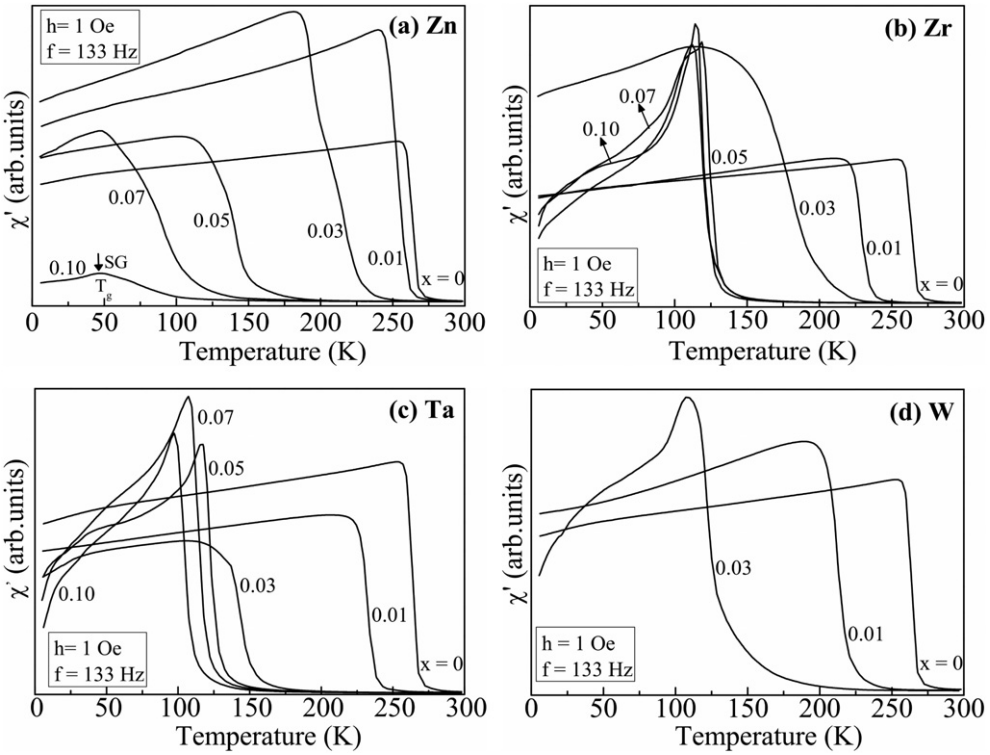

Figure 8. Temperature dependence of in-phase component of ac susceptibility ($\chi'(T)$) in an ac probe field (h) of 1 Oe and an excitation frequency (f) of 133 Hz of $La_{0.67}Ca_{0.33}Mn_{1-x}M_xO_3$ ($0 \leqslant x \leqslant 0.10$) compounds where (a) M = Zn, (b) Zr, (c) Ta and (d) W. $La_{0.67}Ca_{0.33}Mn_{0.90}Zn_{0.10}O_3$ undergoes a spin-glass (SG) transition and the arrow (↓) marks the spin freezing temperature (T_g) of the compound (a). Refer to the text for details.

the former case, a cusp seen in the ac susceptibility at ∼45 K has been taken as the spin freezing temperature (T_g) (marked by an arrow in figure 8(a)). Moreover, T_g is found to shift to higher temperatures with increasing frequency of the ac probe field [55] and the estimated frequency shift of T_g per decade of frequency ∼0.01 agrees well with the typical values for the canonical SG systems [58]. This observation finds additional support from the non-linear ac susceptibility and magnetic relaxation studies and the results will be published elsewhere [59].

4. Discussion

The ionic radius (IR) of Zn^{2+}, Zr^{4+}, Ta^{5+} and W^{6+} for the co-ordination number six is 0.74 Å, 0.72 Å, 0.64 Å and 0.60 Å respectively [60]. Taking the IR alone into account, substitution of Ta^{5+} at the Mn site is not expected to introduce much unit cell and local structural modification and W^{6+} is expected to decrease the unit cell parameters, whereas substitution of Zr^{4+} and Zn^{2+}, with their IRs being comparable, is expected to introduce similar increase in the lattice parameters and corresponding local structural modifications commensurate with their larger IR. Our study shows that Ta^{5+} and W^{6+} substitution expands the unit cell. Not only that, but W^{6+} substitution results in a larger unit cell expansion compared to that of the Ta^{5+} substituted compounds. Zn substitution results in a marginal decrease in the unit cell parameters. Also, the observed unit cell expansion of the Ta^{5+} substituted compounds is comparable to that of Zr^{4+}

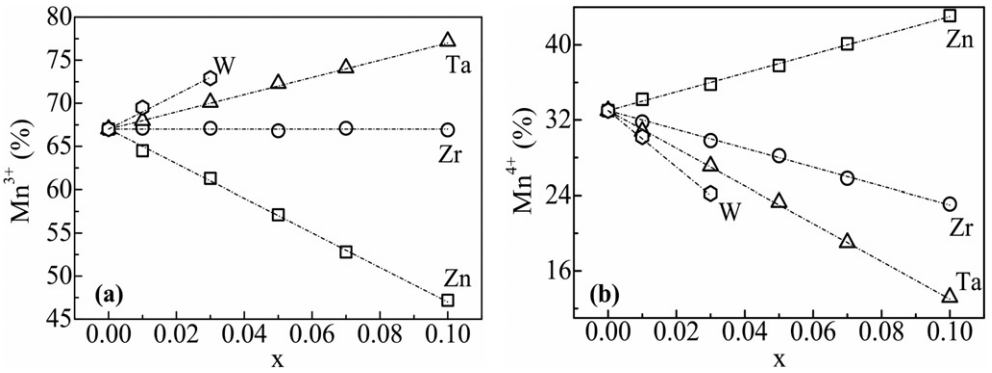

Figure 9. Variation of the relative concentration of (a) Mn^{3+} and (b) Mn^{4+} (in %) as a function of x of $La_{0.67}Ca_{0.33}Mn_{1-x}M_xO_3$ ($0 \leqslant x \leqslant 0.10$) compounds where M = Zn (□), Zr (○), Ta (△) and W (⬡). The dashed line shows the expected variation of the relative concentration of Mn^{3+} and Mn^{4+} based on the charge neutrality. Error bars are smaller than symbols.

substitution of similar compositions. This apparent contradiction in the unit cell dependence is to be understood in terms of the decrease/increase in the average Mn radius ($\langle IR_{Mn} \rangle$) caused by the changes in the average valence of Mn. In this context, two effects are expected on the partial replacement of Mn by elements differing in their valence state in order to preserve the charge neutrality: either an oxidation (reduction) from $Mn^{3+}(Mn^{4+})$ to $Mn^{4+}(Mn^{3+})$ for the divalent (tetra/penta/or hexa-valent) ions, retaining the oxygen stoichiometry, or the formation of the oxygen vacancies in the lattice for the divalent ion and excess oxygen for the tetra-, penta- and hexavalent substituents. If the changes in the oxygen stoichiometry were the dominant mechanism, it is expected that divalent Zn substitution would increase and tetra-/penta- and hexavalent substitutions decrease the unit cell parameters [61]. On the contrary, decrease in unit cell parameters is observed for the Zn substituted compounds and Zr, Ta and W substituted compounds show significant increases in that order. Hence the possibility of the changes in the oxygen stoichiometry is ruled out. Furthermore, Rietveld analysis of the XRD patterns clearly established that while the lower valence state Zn^{2+} substitution results in an increase of Mn^{3+} concentration (figure 9(a)), higher valence state Zr^{4+}, Ta^{5+} and W^{6+} substitutions decrease it, in that sequence. Thus, it is believed that the first mechanism is operative in the present case.

Taking the charge neutrality into consideration, it is expected that tetravalent Zr, pentavalent Ta and hexavalent W strongly shift the average Mn valence towards 3+ as shown in figure 10. While tetravalent Zr decreases only the Mn^{4+} concentration according to $La^{3+}_{0.67}Ca^{2+}_{0.33}Mn^{3+}_{0.67}Mn^{4+}_{0.33-x}Zr^{4+}_{x}O^{2-}_{3}$, Ta^{5+} and W^{6+} not only decrease the Mn^{4+} concentration, but also increase the Mn^{3+} concentration. The difference between the Ta^{5+} and W^{6+} can be explained by the fact that W, due to its hexavalent character introduces *twice as many electrons per atom* as pentavalent Ta according to $La^{3+}_{0.67}Ca^{+}_{0.33}Mn^{3+}_{(0.67+2x)}Mn^{4+}_{(0.33-3x)}W^{6+}_{x}O^{2-}_{3}$ and $La^{3+}_{0.67}Ca^{2+}_{0.33}Mn^{3+}_{(0.67+x)}Mn^{4+}_{(0.33-2x)}Ta^{5+}_{x}O^{2-}_{3}$ respectively. On the other hand, Zn^{2+} substitution decreases (increases) the $Mn^{3+}(Mn^{4+})$ concentration and shifts the average Mn valence *towards 4+* as $La^{3+}_{0.67}Ca^{2+}_{0.33}Mn^{3+}_{(0.67-2x)}Mn^{4+}_{(0.33+x)}Zn^{2+}_{x}O^{2-}_{3}$. These observations find a close agreement with the detailed powder XRD studies carried out using the GSAS Rietveld program. From the Rietveld studies, the concentration of Mn^{4+} is estimated and its variation with concentration of substituent is shown in figure 9(b). A close agreement is seen between the estimated Mn^{4+} concentration from the refinement program (open symbols) and the one

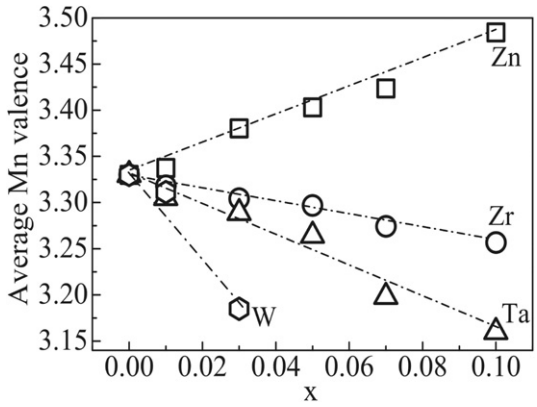

Figure 10. Composition dependence of average Mn valence calculated from the refined Mn^{3+}, Mn^{4+} and M concentration of $La_{0.67}Ca_{0.33}Mn_{1-x}M_xO_3$ ($0 \leqslant x \leqslant 0.10$) compounds where M = Zn (□), Zr (○), Ta (△) and W (⬡). The dotted line is the one predicted based on the charge neutrality consideration. Refer to the text for details.

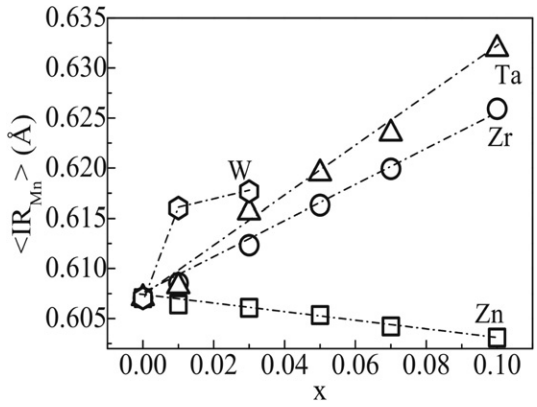

Figure 11. Average Mn radius ($\langle IR_{Mn}\rangle$) versus composition (x) of $La_{0.67}Ca_{0.33}Mn_{1-x}M_xO_3$ ($0 \leqslant x \leqslant 0.10$) compounds where (a) M = Zn, (b) Zr, (c) Ta and (d) W. The open symbols and dotted line denote $\langle IR_{Mn}\rangle$ calculated from the refined relative concentration of Mn^{3+}, Mn^{4+} and M ions and the predicted one based on the charge neutrality consideration respectively.

predicted based on the foregoing charge neutrality consideration (dotted line). Thus, the shift of the average valence state of the Mn ion to 3+ (4+) (figure 10) is expected to bring out an increase (decrease) in the average Mn ionic radius (figure 11) and an associated increase (decrease) in the lattice parameters (figure 3). Thus, the observed unit cell expansion (contraction) is essentially due to an increase (decrease) in $\langle IR_{Mn}\rangle$ upon Zr, Ta and W (Zn) substitution even though it must be noticed that the electronic state also influences the volume of the unit cell.

Comparing the zero field $\rho(T)$ (figure 5) and $\chi'(T)$ (figure 8) data, the following observations are made. Except for $x = 0.10$ of Zn, all the other compounds, including those not exhibiting an MIT, show a para- to ferromagnetic transition. A close matching (within ±5 K) between T_c and T_{MI} is observed for $x < x_c$, beyond which there is either a discernable difference between T_c and T_{MI} or T_{MI} vanishes. In general, the variation of T_c with the concentration of the substituents of the present study is non-linear—an initial strong

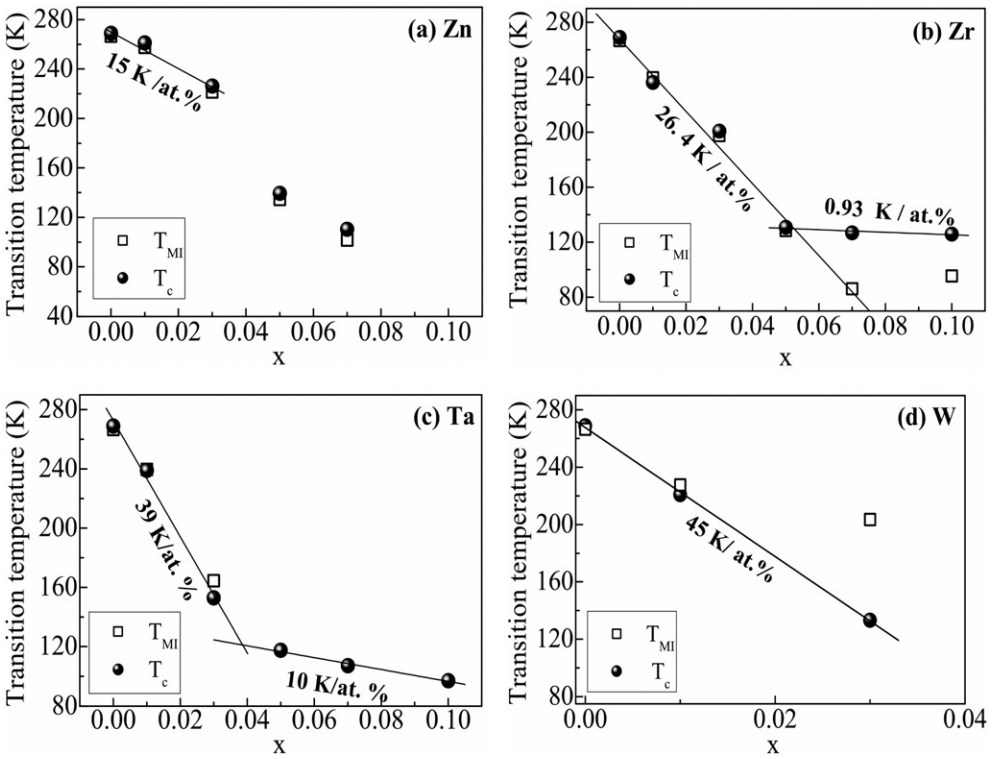

Figure 12. Variation of metal–insulator transition temperature (T_{MI}) and Curie temperature (T_c) as a function of composition (x) of $La_{0.67}Ca_{0.33}Mn_{1-x}M_xO_3$ ($0 \leqslant x \leqslant 0.10$) compounds where (a) M = Zn, (b) Zr, (c) Ta and (d) W. Straight lines are the best fit to the experimental data to estimate the rate of suppression in the transition temperatures.

decrease up to x_c followed by a weak decrease. The initial decrease is fitted to a straight line and the corresponding suppression rate, dT_c/dx ($\sim dT_{MI}/dx$) is estimated and is shown in figure 12. While the divalent Zn substitution decreases the transition temperatures at a rate of 15 K/at.%, tetravalent Zr substitution results in an enhanced suppression rate $\sim$ 26 K/at.%. Still higher suppression rates of $\sim$39 and $\sim$45 K/at.% are observed for the pentavalent Ta and hexavalent W substituted systems respectively. In passing, it is worth mentioning that the suppression rate of $\sim$45 K/at.% for the W^{6+} system is the largest reported for the Mn site substituted $La_{0.67}Ca_{0.33}MnO_3$.

From the XRD studies, it is seen that all the substituents, depending on their valence state, alter the average Mn valence either towards 3+ or 4+ to preserve the charge neutrality. Such a shift leads to changes in the majority charge carrier concentration (CCC). The rate of shift of average valence state of Mn increases with Zr^{4+}, Ta^{5+} and W^{6+} in that order (figure 10). This arguably mimics the trend observed for dT_c/dx. From the present studies, it is not possible to confirm whether reduction in the majority CCC is a dominant cause for the observed suppression rate. If CCC is a dominant factor affecting transport and magnetic properties, the effect should also be seen in $La_{1-z}Ca_zMnO_3$ compounds [3, 62] with comparable Mn^{4+} concentration as the present Zr^{4+}, Ta^{5+}, W^{6+}(Zn^{2+}) substituted $La_{0.67}Ca_{0.33}MnO_3$. For an inter-comparison, such curves are displayed in figure 13. In all cases, the substituted compounds exhibit much lower values of T_c. For instance, for $x = 0.05$, the relative

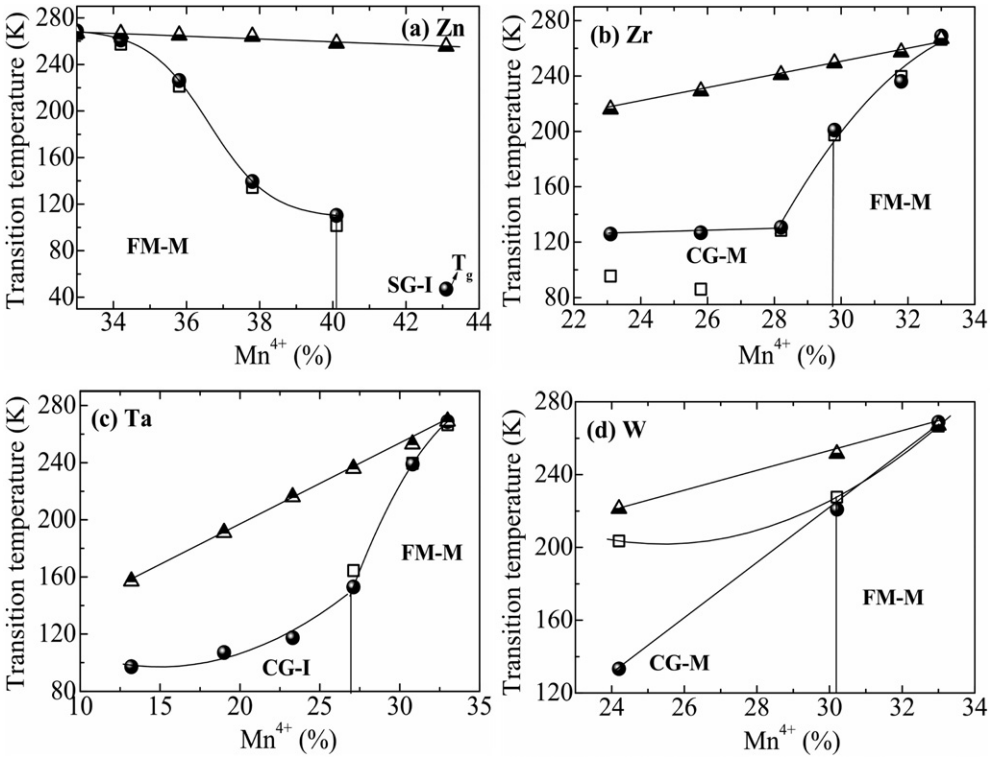

Figure 13. Phase diagram of $La_{0.67}Ca_{0.33}Mn_{1-x}M_xO_3$ ($0 \leqslant x \leqslant 0.10$) compounds where (a) M = Zn, (b) Zr, (c) Ta and (d) W as a function of relative concentration of Mn^{4+} (%) observed. FM-M, FM-I, CG-M, CG-I and SG-I denote ferromagnetic–metal, ferromagnetic–insulator, metallic–cluster glass, cluster glass–insulator and spin glass–insulator respectively of the substituted compounds. T_g (a) denotes the spin freezing temperature. Refer to the text for the details. For an intercomparison, a similar plot for $La_{1-z}Ca_zMnO_3$ compounds (▲) (reproduced from [3]) with the same Mn^{4+} concentration as that of substituted compounds is also given. The solid line is only a guide to the eye.

concentration of Mn^{4+} for Ta is ∼23.3%, leading to a T_c of ∼117 K and low temperature glassy behaviour. On the other hand, ferromagnetism and metallicity are found in $La_{0.77}Ca_{0.23}MnO_3$ ($T_c \sim 220$ K) with the same Mn^{4+} concentration as in $x = 0.05$ of Ta [62]. Therefore, the effect of carrier density seems to be insufficient to account for the strong reduction in the transition temperatures observed in the present case. The difference also cannot be rationalized in terms of local magnetic coupling effects, as the substituents are diamagnetic in nature and are not expected to introduce such an effect. As explained above, $\langle IR_{Mn} \rangle$ is substantially modified with substitution. This strongly induces local structural modifications, which plays a significant role in the reduction of the transition temperatures. As presented in figures 4(a) and (b), unlike the case of Zn^{2+}, all the other substituents introduce larger structural modification: a significant increase in $\langle d_{Mn-O} \rangle$ and a substantial decrease of ⟨Mn–O–Mn⟩. These two modifications are expected to decrease the DE interaction strength, similar to what has been observed in the rare-earth site substituted manganites [63]. Thus a reduction in the transition temperatures, depending upon the extent of $\langle d_{Mn-O} \rangle$ and ⟨Mn–O–Mn⟩ modification, would result. This being so, Zr^{4+} and Ta^{5+} bring out local structural modification of almost comparable magnitude involving the elongation of $\langle d_{Mn-O} \rangle$ and a substantial reduction of ⟨Mn–O–Mn⟩. If the local

structural effects were the dominant factor, it is expected that Zr^{4+} and Ta^{5+} would decrease the transition temperatures to almost the same extent. On the other hand, Ta^{5+} had not only resulted in larger reduction of the transition temperatures, ∼39 K/at.%, but also modified the ground state to a glassy insulator even at lower concentration of substitution (beyond 3 at.%) compared to that of Zr^{4+} substituted ones. Hence another effect seems to be necessary to understand the variations in dT_c/dx and significantly larger reduction in the transition temperatures for the Ta^{5+} and W^{6+} substituted compounds.

As pointed out by Alonso *et al* [64], the changes in the charge state at the Mn site may create a *random electrostatic potential* that scatters the charge carriers. Taking the electrostatic potential into account, calculation by these authors indicates enhanced suppression of the transition temperatures and appearance of glassy ground states. Due to the large positive charge of Ta^{5+} and W^{6+}, one would expect a strong electrostatic effect for these cases. It is expected that this mechanism adds to the unusually strong suppression of the itinerant DE ferromagnetism and leads to the largest reduction of the transition temperatures. The following important features in the transport and the magnetic properties of Zr and W substituted compounds, however, need a special mention. For W substituted compound with $x = 0.03$, MIT ($T_{MI} \sim 203$ K) occurs at temperatures much above the Curie temperature ($T_c \sim 133$ K). T_{MI} is well above T_c for $x = 0.07$ and 0.10 of Zr substituted compounds. It is even more surprising that MIT shifts to higher temperature for $x = 0.10$ of Zr instead of the as expected low temperature shift with increasing x. Fitting of XRD patterns conforming to orthorhombic *Pnma* symmetry with no peaks left un-indexed and also with the systematic increase in the unit cell parameters rule out insolubility of Zr as being the cause of the observed high temperature shift of T_{MI}. Similar behaviour is also reported in the layered manganite of type $La_{1.4}Sr_{1.6-y}Ba_yMn_2O_7$ for higher concentration of Ba [65] and the authors suggest that such an anomalous behaviour might be due to the correlation between the spin clusters and the percolative transport in those compounds.

5. Summary

All substitutions, excluding W^{6+} beyond $x = 0.03$, form solid solutions in the entire range of substitution. Although the substitution has left the crystal symmetry unaltered, the unit cell parameters are found to change to various extents. The difference in the unit cell dependence and the enhanced local structural modification with substitution in the order Zn^{2+}, Zr^{4+}, Ta^{5+} and W^{6+} are understood in terms of the increase (decrease) in the average Mn radius due to Zr, Ta, W (Zn) substitution caused by the changes in the average valence of Mn. Both T_{MI} and T_c are found to decrease with substitutions, but to different extents. This study demonstrates that pentavalent and hexavalent substitutions not only reduce the transition temperatures to the largest extent reported for the Mn site substituted manganites but also induce cluster-glass behaviour at very low concentration ($x \sim 0.05$ and 0.03 for Ta^{5+} and W^{6+} ions respectively) compared to that of other divalent, trivalent or tetravalent substitutions for Mn in the ferromagnetic–metallic $La_{0.67}Ca_{0.33}MnO_3$. Besides modification of majority carrier concentration due to the increased (decreased) Mn^{3+} concentration and enhanced local structural effects, the local electrostatic potential due to the deviating charge state of the substituent at the Mn site seems to be certainly important and accounts for the unusually strong reduction in the itinerant ferromagnetism and the observed glassy states of the compounds. As a final point, one more remark should be made in regard to the conclusions reached in this study. The effect of random electrostatic potential due to the local charge variations in the La site substituted ions is shown to have no significant effect on the transition temperatures and the ground state properties of the compounds. Our study, on the other hand, proposes that, unlike

the case of rare-earth site substituted manganites, the charge state modification at the Mn site is the most deleterious for the FM-M ground state of CMR manganites.

Acknowledgments

This work is supported by DFG, FOR520, Germany. One of the authors, LSL, also thanks the Council of Scientific and Industrial Research (CSIR), India, for a Senior Research Fellowship.

References

[1] Jin S, Tiefel T H, McCormack M, Fastnacht R A, Ramesh R and Chen L H 1994 *Science* **264** 413
[2] Jonker G H and Van Santeen J H 1950 *Physica* **16** 337
[3] Cheong S W and Hwang H Y 2000 *Colossal Magnetoresistive Oxides* ed C N R Rao and Y Tokura (India: Gordon and Breach Science) p 237
[4] Zener C 1951 *Phys. Rev.* **82** 403
[5] Hwang H Y, Cheong S-W, Radaelli P G, Marezio M and Batlogg B 1995 *Phys. Rev. Lett.* **75** 914
[6] Millis A J 1998 *Nature* **392** 147
[7] Millis A J, Littlewood P B and Shraiman B I 1995 *Phys. Rev. Lett.* **74** 5144
[8] Chen C H and Cheong S-W 1996 *Phys. Rev. Lett.* **76** 4042
[9] Snyder J F, Hiskes R, DiCarolis S, Beasley M R and Geballe T H 1996 *Phys. Rev.* B **53** 14434
[10] Jaime M, Salamon M B, Rubinstein M, Treece R E, Horwitz J S and Chrisey D B 1996 *Phys. Rev.* B **54** 11914
[11] Jaime M, Salamon M B, Rubinstein M, Dorsey P and Emin D 1997 *Phys. Rev. Lett.* **78** 951
[12] Babushkina N A, Taldenkov A N, Belova L M, Chistotina E A, Yu Gorbenko O, Kaul A R, Kugel K I and Khomskii D I 2000 *Phys. Rev.* B **62** R6081
[13] Coey J M D, Viret M, Ranno L and Qunadjela K 1995 *Phys. Rev. Lett.* **75** 3910
[14] Sheng L, Xing D Y, Sheng D N and Ting C S 1997 *Phys. Rev.* B **56** R7053
[15] Dagotto E, Hotta T and Moreao A 2001 *Phys. Rep.* **344** 1 and references therein
[16] Moreo A, Mayor M, Feiguin A, Yunoki S and Dagotto E 2002 *Phys. Rev. Lett.* **84** 5568
[17] Uehara M, Mori S, Chen C H and Cheong S-W 1999 *Nature* **399** 560
[18] Fäth M, Freisem S, Menovsky A A, Tomioka Y, Aarts J and Mydosh J A 1999 *Science* **285** 1540
[19] Dagotto E 2005 *New J. Phys.* **7** 67
[20] Freitas R S, Ghivelder L, Damay F, Dias F and Cohen L F 2001 *Phys. Rev.* B **64** 144404
[21] Terai T, Kakeshita T, Fukuda T, Saburi T, Takamoto N, Kindo K and Honda M 1998 *Phys. Rev.* B **58** 14908
[22] de Teresa J M, Ritter C, Ibarra M R, Algarabel P A and Marquina C 1996 *J. Phys.: Condens. Matter* **8** 7427
[23] Hwang H Y, Cheong S-W, Radaelli P G, Marezio M and Batlogg B 1995 *Phys. Rev. Lett.* **75** 914
[24] Rodriguez-Martínez L M and Attfield J P 1996 *Phys. Rev.* B **54** R15622
[25] Rodriguez-Martínez L M and Attfield J P 2000 *Phys. Rev.* B **63** 024424
[26] Rodriguez-Martínez L M and Attfield J P 1998 *Phys. Rev.* B **58** 2426
[27] de Teresa J M, Ibarra M R, García J R, Blasco J, Ritter C, Algarabel P A, Marquina C and del Moral A 1996 *Phys. Rev. Lett.* **76** 3392
[28] Maignan A, Martin C, Van tendeloo G, Hervieu M and Raveau B 1999 *Phys. Rev.* B **60** 15214
[29] de Teressa J M, Ritter C, Ibarra M R, Algarabel P A, Garcia-Munoz J L, Blasco J, Garcia J and Marquina C 1997 *Phys. Rev.* B **56** 3317
[30] Williams A J, Sobotka B M and Attfield J P 2003 *J. Solid State Chem.* **173** 456
[31] Attfield J P 2002 *Cryst. Eng.* **5** 427
[32] Liu X, Xu X and Zhang Y 2000 *Phys. Rev.* B **62** 15112
[33] Awana V P S, Schmitt E, Gmelin E, Gupta A, Narlikar A V, De Lima O F, Cardoso C A, Malik S K and Yelon W B 2000 *J. Appl. Phys.* **87** 5034
[34] Yuan L, Zhu Y and Ong P P 2001 *Solid State Commun.* **120** 495
[35] Rivadulla F, López-Quintela M A, Hueso L E, Sande P and Rivas J 2000 *Phys. Rev.* B **62** 5678
[36] Rubinstein M, Gillespie D J, Snyder J E and Tritt T M 1997 *Phys. Rev.* B **56** 5412
[37] Ahn K H, Wu X W, Liu K and Chien C L 1996 *Phys. Rev.* B **54** 15299
[38] Blasco J, Garcia J, de Teressa J M, Ibarra M R, Perez J, Algarabel P A and Marquina C 1997 *Phys. Rev.* B **55** 8905
[39] Turilli G and Licci F 1996 *Phys. Rev.* B **54** 13052
[40] Sanchez M C, Blasco J, García J, Stankiewicz J, de Teressa J M and Ibarra M R 1998 *J. Solid State Chem.* **138** 226

[41] Sun Y, Xu X, Zheng L and Zhang Y 1999 *Phys. Rev.* B **60** 12317
[42] Przewoźnik J, Chmist J, Kolwicz-Chodack L, TarNawski Z, Kołodzieczyk A, Krop K, Kellner K and Gritzner G 2004 *Acta Phys. Pol.* A **106** 665
[43] Sun J R, Rao G H, Shen B G and Wong H K 1998 *Appl. Phys. Lett.* **73** 2998
[44] Seetha Lakshmi L, Sridharan V, Natarajan D V, Sastry V S and Radhakrishnan T S 2001 *J. Phys.–Pramana* **58** 1019
[45] Seetha Lakshmi L, Sridharan V, Natarajan D V, Rawat R, Chandra S, Sastry V S and Radhakrishnan T S 2004 *J. Magn. Magn. Mater.* **279** 41
[46] Larson A C and von Dreele R B 2000 *Los Alamos National Laboratory Report* LAUR 86-748
[47] Lufaso M W and Woodward P M 2001 *Acta Crystallogr.* B **57** 725
[48] Emin D and Holstein T 1969 *Ann. Phys.* **53** 439
[49] Jaime M, Salamon M B, Rubinstein M, Treece R E, Horwitz J S and Chrisey D B 1997 *Phys. Rev.* B **54** 11914
[50] Hwang H W, Cheong S-W, Ong N P and Batlogg B 1996 *Phys. Rev. Lett.* **77** 2041
[51] Raychaudhuri P, Sheshadri K, Taneja P, Bandyopadhyay S, Ayyub P, Nigam A K, Pinto R, Chaudhary S and Roy S B 1999 *Phys. Rev.* B **59** 13919
[52] Kozlova N, Dörr K, Eckert D, Walter T and Műller K-H 2003 *J. Magn. Magn. Mater.* **261** 48
[53] Mahendiran R and Raychaudhuri A K 1996 *Phys. Rev.* B **54** 16044
[54] Rao G H, Sun J R, Kattwinkel A, Haupt L, Bärner K, Schmitt E and Gmelin E 1999 *Physica* B **269** 379
[55] Seetha Lakshmi L 2005 Mn site substituted $La_{0.67}Ca_{0.33}MnO_3$ ortho-perovskites: role of charge state, local structure and local spin coupling on the ground state properties *PhD Thesis* University of Madras, Chennai, India
[56] Seetha Lakshmi L, Dörr K, Nenkov K, Handstein A, Müller K-H and Sastry V S 2007 *J. Phys.: Condens. Matter* **19** 216218
[57] Cai J-W, Wang C, Shen B-G, Zhao J-G and Zhan W-S 1997 *Appl. Phys. Lett.* **71** 1727
[58] Mydosh J A 1993 *Spin Glasses: an Experimental Introduction* (London: Taylor and Francis)
[59] Seetha Lakshmi L and Nigam A K 2007 private communication
[60] Shannon R D and Prewitt C T 1976 *Acta Crystallogr.* A **32** 751
[61] Malavasi L, Mozzati M C, Azzoni C B, Chiodelli G and Flor G 2002 *Solid State Commun.* **123** 321
[62] Schiffer P, Rameriz A P, Bao W and Cheong S-W 1995 *Phys. Rev. Lett.* **75** 3336
[63] Radaelli P G, Marezio M, Hwang H Y, Cheong S-W and Batalogg B 1996 *Phys. Rev.* B **54** 8992
[64] Alonso J L, Fernández L A, Guinea F, Laliena V and Martín-Mayor V 2002 *Phys. Rev.* B **66** 104430
[65] Zhu H, Zhu D L and Zhang Y H 2002 *J. Appl. Phys.* **92** 7355